Geophysical Journal International

Geophys. J. Int. (2023) **234,** 585–596
Advance Access publication 2023 February 27
GJI Geodynamics and Tectonics

https://doi.org/10.1093/gji/ggad077

Analytical computation of total topographic torque at the core–mantle boundary and its impact on tidally driven length-of-day variations

M. Puica,[1,2,3] V. Dehant,[1,4] M. Folgueira,[2] T. Van Hoolst[1] and J. Rekier[1]

[1] *Royal Observatory of Belgium, Reference Systems and Planetology Division, B*-1180 *Brussels, Belgium. E-mail: veronique.dehant@oma.be*
[2] *Universidad Complutense de Madrid, Faculty of Mathematical Science,* 28040 *Madrid, Spain*
[3] *University of Oslo, Faculty of Mathematics and Natural Sciences, N*-0315 *Oslo, Norway*
[4] *Université catholique de Louvain, B*-1348 *Louvain-la-Neuve, Belgium*

Accepted 2023 January 30. Received 2023 January 29; in original form 2022 July 11

SUMMARY

The Earth's rotation exhibits periodic variations as a result of gravitational torques exerted by the Sun and the Moon and of angular momentum exchange of the solid Earth with the Earth's atmosphere and hydrosphere. Here, we aim at determining the complementary effect of the deep interior on variations in the length-of-day (LOD) and focus on the influence of topography at the core–mantle boundary (CMB). For this purpose, we have developed an analytical approach for solving the Navier–Stokes equation for global rotational motions and inertial waves, based on and extending the approach of Wu & Wahr (1997). An advantage of the analytical approach is that it allows to identify the frequencies and topographic spherical harmonics degrees and orders where resonance can happen, as well as to quantify the total amplifications in the tidal effects on LOD variations. Although the resonances are found to be sometimes quite near tidal frequencies, we show that they are not sufficiently close to induce significant perturbations in LOD variations, except for two of the tides, the fortnightly and monthly tides M_f and M_m. Our results go beyond the findings of Wu & Wahr (1997), extending them to a much wider range of degrees and orders of topographic coefficients. We show that there is an amplification in M_f and M_m induced by the degree 18-order 10 and by the degree 7-order 1 of the topography, respectively. Our approach is generic in the sense that it can be applied to other orientation changes of the Earth as well as to other planets.

Key words: Earth rotation variations; Core; Planetary interiors.

1 INTRODUCTION – MOTIVATION

Hide (1969) showed that topography at the core–mantle boundary (CMB) of the order of a couple of kilometres affects long-period length-of-day (LOD) variations. In his pioneering work and in the subsequent improved studies (e.g., Hide 1989; Hide *et al*. 1993; Jault and Le Mouël 1989; 1990; Yoshida and Hamano 1993; 1995; Kuang and Bloxham 1993; Zatman and Bloxham 1997; 1999; Kuang and Chao 2001; Buffett 1996; Greiner-Mai *et al*. 2003; Mound and Buffett 2003; Gillet *et al*. 2010, 2017, 2019, 2022a, 2022b; Asari and Wardinski 2015; Teed *et al*. 2018; Gerick *et al*. 2020), the focus was on the pressure torque at the CMB from core flow at long timescale (secular variations and long-term motions related to the magnetic field) in order to compute the core contribution to LOD variations at decadal timescale. At those long timescales, the Coriolis and pressure forces are dominant inside the fluid core, with the magnetic (Lorentz) and buoyancy forces completing the balance of forces (the so-called MAC balance; Aubert & Gillet 2021). On shorter annual and (sub)seasonal timescales considered here, inertia is thought to dominate over the buoyancy and Lorentz forces. The most important core modes for LOD are then the inertial modes, for which Coriolis plays the role of a restoring force (for a review of these oscillations, see Triana *et al.* 2022).

In the present paper, we study **tidal effects** on **short timescale (seasonal, months, days)**. Observations of LOD variations as provided by Global Navigation Satellite System (GNSS) and/or Very Long Baseline Interferometry (VLBI) and corrected for the atmospheric, oceanic and possibly hydrological effects show unexplained residuals at the level of ten to a few tens of microseconds for periods corresponding to the tidal periods around 2 weeks or 1 month (see e.g. Kouba and Vondrák 2005; Böhm *et al.* 2010; Senior *et al.* 2010; Ray *et al.* 2013; Rebischung *et al.*, 2016; Watkins *et al.* 2018; Landskron & Böhm 2019). This questions the accuracy of the tidal corrections in LOD and provides a motivation for our work. Analyses of the present-day data of LOD variations at short timescale often concentrate on effects from

the surface geophysical fluids (e.g. Chen 2005; Zhou *et al.* 2006; Jin *et al.* 2011; Marcus *et al.* 2012; Lambert *et al.* 2017; Dill & Dobslaw 2019; Chen *et al*. 2019), as these explain the most important part of the seasonal changes in LOD. Here, we study the possible effects of the core. We assess the importance of inertial waves inside the core for LOD variations and quantify the effects of the associated core flows in the presence of a CMB topography on the total pressure torque at the CMB in the frame of tidal effects on LOD. We will examine whether topography at the CMB may explain the observed residuals.

Tidal effects are computed by evaluating the Earth's deformations (including global rotational deformations) in response to a gravitational tidal potential. In this procedure, the Earth is usually considered, at initial state, as an ellipsoid in hydrostatic equilibrium. In such a biaxial ellipsoid, zonal flows associated with the Earth's rotation variations are not affecting the Earth's tidal response if the core is assumed to be inviscid. The Poincaré flow, which is to lowest-order approximation a rotation around an axis in the equator, does not play any direct role in LOD variations. CMB topography changes this situation by creating a non-zero pressure torque in the polar direction at the CMB and transfer of angular momentum between core and mantle. The torque depends on the inertial modes in the core, which can cause resonance effects in LOD. Given that the topography at the CMB can be developed in spherical harmonics (SH) truncated at a certain degree (corresponding to the smallest wavelength), we will derive an expression of the torque at the CMB that involves the coefficients of the development of the topography in SH. The effect on LOD will be shown to also depend on the amplitudes of the topographical SH and on the presence of resonances with inertial modes in the liquid core.

The philosophy of our computation follows Wu & Wahr (1997), who computed the effects of the topography on LOD and nutations. For CMB topography developed up to degree 6, they showed that this effect can be significant and can be of the level of 1 mas on the annual retrograde nutation, which is more than 12 per cent of the total non-rigid contribution of 8 mas. This value corresponds to the difference between the observed retrograde annual nutation amplitude, 33 mas (Herring *et al.* 2002), and the value computed for a rigid Earth, 25 mas. When considering a flattened Earth in hydrostatic equilibrium, this nutation amplitude takes the value of 31.1 mas (adding 6.1 mas to the rigid Earth value) (Wahr 1981). Mathews *et al.* (1991a, 1991b, 2002) could explain the residual 1.9 mas considering a non-hydrostatic flattening for the core and electromagnetic coupling. A topography effect at the level of 1 mas would be more than half of these effects, while the hydrostatic/non-hydrostatic effect is at the first order and the topography at the second order in the small quantities such as the normalized topography amplitudes. This large 1 mas topography effect found by Wu & Wahr (1997) is difficult to reconcile with the observations, unless the topography amplitudes are much smaller than the values at the level of 3.5 km that Wu & Wahr (1997) used. The topography contributions to the other nutation amplitudes were not computed in the paper of Wu & Wahr (1997). These are additional reasons for revisiting the CMB topography contribution to Earth rotation and orientation changes.

In view of the uncertainties in the CMB topography coefficients and to facilitate the physical interpretation of the complex mathematical developments, we establish a theory that is completely analytical. The method consists in separating the Navier–Stokes equation into two equations whose solutions for the fluid motions can be computed analytically. This separation is performed so that one part describes the most important classical global rotational motions and the other part the smaller additional inertial motions. Both parts of the velocity field are assumed to be incompressible flows. The no-penetration boundary conditions imposed at the CMB yield a relation involving the additional velocity field and the CMB topography. This allows to solve for the coefficients appearing in the expression of the additional velocity field in terms of the topography coefficients and to estimate resonance effects for the frequencies involved in the tidal forcing.

The paper is structured as follows. In Section 2, on the mathematical model, we first recall the Liouville equations for the global rotation and their solutions (Section 2.1). We then describe the way to obtain the topographic coupling for tidal LOD variations (Section 2.2). Section 2.3 deals with the analytical solutions of the equations for both the global rotation part and the incremental part of the velocity field related to the inertial waves. We detail the solutions for the incremental velocity and provide the expressions for the topography used in the equations. In Section 3, we further develop and solve the equations of the topographic coupling for a two-layered Earth model and we come up with a new transfer function for tidal changes in LOD. Section 4 provides the concluding remarks.

2 MATHEMATICAL MODEL

2.1 Equations of motion in the frame of rotational dynamics

Since we want to assess the effect of topographical coupling at the CMB on LOD variations, we can safely neglect Earth's solid inner core in our study. The Liouville equations governing the rotation of the two-layer Earth model can be written as (Sasao *et al.* 1980):

$$\frac{\partial \mathbf{L}}{\partial t} + \Omega \times \mathbf{L} = \Gamma, \tag{1}$$

$$\frac{\partial \mathbf{L}_f}{\partial t} - \boldsymbol{\omega}_f \times \mathbf{L}_f = \Gamma_{\rm cmb}, \tag{2}$$

where Ω is the rotation vector of the solid mantle and $\boldsymbol{\omega}_f$ the differential rotation vector of the liquid core with respect to the mantle. The rotation vector of the core can thus be written as $\Omega+\boldsymbol{\omega}_f$. $\mathbf{L}$ and $\mathbf{L}_f$ denote the angular momentum of the whole Earth and liquid core, respectively. The quantity, Γ, represents the torque exerted on the planet by external sources (primarily the Sun and Moon). $\Gamma_{\rm cmb}$ is crucial to the present study. It represents the part of the torque caused by the mantle on the liquid core that comes in addition to the external gravitational torque acting on the liquid core and the torque caused by the fluid pressure on an hydrostatic oblate mantle (see again Sasao *et al.* 1980, and

Dehant & Mathews 2015, see also Rekier *el al.* 2020). This torque includes the electromagnetic torque and the drag on the viscous torque, but we don't consider those contributions here and keep only the pressure torque related to the topography of the CMB in order to be able to evaluate its effect independently from the other physical mechanisms.

Following the standard procedure, we choose the mean axis of rotation as our polar z-axis, and write the deviations of the Earth and liquid core from steady rotation as:

$$\Omega = \Omega_0(\hat{\mathbf{z}} + \mathbf{m}), \tag{3}$$

$$\boldsymbol{\omega}_f = \Omega_0 \mathbf{m}_f, \tag{4}$$

where $\mathbf{m}$ and $\mathbf{m}_f$ are small dimensionless quantities and Ω_0 the mean mantle angular velocity of rotation. To first order in the small quantities, the components of the Liouville equations along the rotation axis decouple from those in the equatorial directions. For a single component of the external torque with frequency $\omega_{\rm tidal} = \sigma_m \Omega_0$, as measured in the inertial frame, the third, or polar, components of eqs (1) and (2) (Dehant & Mathews 2015) write:

$$\mathrm{m}_3 + \frac{c_{33}}{C} + \frac{C_f}{C}\mathrm{m}_{f,3} = -\frac{i\Gamma_3}{C\sigma_m\Omega_0^2}, \tag{5}$$

$$\mathrm{m}_3 + \mathrm{m}_{f,3} + \frac{c_{f,33}}{C_f} = -\frac{i\Gamma_{\rm cmb,3}}{C_f\sigma_m\Omega_0^2}, \tag{6}$$

where C and C_f denote the polar moments of inertia of the Earth and its liquid core, respectively, and c_{33} and $c_{f,33}$ are the increments in these quantities caused by tidal deformations at the frequency considered usually computed using the Love number formalism. Subscripts 3 refer to the polar z component.

The incremental rotation parameter m_3 is related to the change in the LOD, ΔLOD, by

$$\frac{\Delta\mathrm{LOD}}{\mathrm{LOD}} = -\mathrm{m}_3. \tag{7}$$

In the absence of topographic coupling at the CMB ($\Gamma_{\rm cmb,3} = 0$), eqs (5) and (6) can be readily solved, giving:

$$\mathrm{m}_3^0 = -\frac{c_{\mathrm{m},33}}{C_m} - \frac{i\Gamma_3}{C_m\sigma_m\Omega_0^2}, \tag{8}$$

$$\mathrm{m}_{f,3}^0 = -\frac{c_{f,33}}{C_f} - \mathrm{m}_3^0, \tag{9}$$

where $C_m = C - C_f$ and $c_{m,33} = c_{33} - c_{f,33}$ are the mantle moment of inertial and its increment also computed using the Love number formalism. Wu & Wahr (1997) showed that this solution is sufficient to evaluate the topographic torque at the CMB, $\Gamma_{\rm cmb,3}$ and that the Earth's rotational response can be calculated as:

$$\mathrm{m}_3 = \mathrm{m}_3^0 + \frac{i\Gamma_{\rm cmb,3}}{C_m\sigma_m\Omega_0^2}. \tag{10}$$

Wu & Wahr (1997) further showed that $\Gamma_{\rm cmb,\,3}$ exhibits resonances at some particular frequencies, which, according to eqs (7) and (10), also manifest themselves in ΔLOD. We review this procedure in the remainder of this section.

Note that the deformation effects related to the incremental flux due to the existence of a topography are smaller than those related to the main core flow and partly accounted for by considering the induced readjustment of the flow and the associated changes in the moments of inertia through the use of Love numbers specifying the elastic response of the Earth to a unit tidal forcing. The additional $c_{m,33}$ and $c_{f,33}$ can, therefore, be neglected in the lowest order of approximation.

2.2 CMB topography and topographic torque

In seismology, it is common practice to parametrize the CMB surface radius as follows:

$$r_{\rm CMB} = R\left[1 + \sum_{n=1}^{N}\sum_{m=0}^{n}(\varepsilon_{c\,n}^m \cos m\lambda + \varepsilon_{s\,n}^m \sin m\lambda)P_n^m(\cos\theta)\right], \tag{11}$$

where R is the mean radius of the core, θ and λ are the colatitude and longitude, respectively and $P_n^m(\cos\theta)$ denotes the associated Legendre polynomials of (integer) degree n and order m. In the above parametrization, $\varepsilon_{c\,n}^m$ and $\varepsilon_{s\,n}^m$ are real valued parameters. For our purpose, we find it more convenient to use instead:

$$r_{CMB} = R\left[1 + \left(\varepsilon_2^0\right)_{\rm hydrostat.} P_2^0(\cos\theta) + \left\{\sum_{n=1}^{N}\sum_{m=-n}^{m=n}\varepsilon_n^m Y_n^m(\theta,\lambda)\right\}\right] \tag{12}$$

where ε_n^m now are the complex coefficients of the SH $Y_n^m(\theta,\lambda)$ of order n and degree m. These SH are based on the associated Legendre polynomials P_n^m by:

$$Y_n^m(\theta,\lambda) = \sqrt{\frac{2n+1}{4\pi}\frac{(n-m)!}{(n+m)!}}\cdot P_n^m(cos\theta)e^{im\lambda},\ m \geq 0 \tag{13}$$

and $Y_n^{-m}(\theta,\lambda) = (-1)^m (Y_n^{-m})^*(\theta,\lambda)$ with $(Y_n^{-m})^*$ the complex conjugate of Y_n^m. Note that the constant term multiplying P_n^m insures orthonormality of Y_n^m.

The expression of ε_n^m in terms of $\varepsilon_{c,n}^m$ and $\varepsilon_{s,n}^m$ are given in Appendix B. In writing eq. (11), we have explicitly isolated the part of ε_2^0 attributed to the hydrostatic deformation of the CMB surface, so that the set of remaining coefficients $\{\varepsilon_n^m\}$ relates to the non-hydrostatic deformation only.

If we can find a way to compute the pressure inside the fluid core, we may then use the topography expression (12) to compute the pressure torque on the non-hydrostatic part of the CMB topography, which must be equal and opposite in sign to the torque caused by the mantle on the liquid core, by virtue of Newton's third law:

$$\begin{aligned}\Gamma_{\rm cmb} &= \Gamma_{\rm pressure} - \Gamma_{\rm pressure}^{\rm hydrostat.}\\ &= -\oint_{\rm cmb} P(\mathbf{r}\times\hat{\mathbf{n}})\, dS + \oint_{\rm hydrostat.} P\left(\mathbf{r}\times\hat{\mathbf{n}}^0\right)\, dS,\end{aligned} \tag{14}$$

where the first integral runs over the bumpy CMB topography with normal vector $\hat{\mathbf{n}}$ and the second integral runs over the hydrostatic oblate ellipsoid with normal vector $\hat{\mathbf{n}}^0$. In the next section, we explain how to evaluate the pressure by computing the dynamics of the flow inside the liquid core.

2.3 Flow inside the core

In the frame rotating at angular velocity Ω relative to the inertial frame, the inviscid flow inside the liquid core is governed by the momentum equation

$$\frac{\partial \mathbf{V}}{\partial t} + (\mathbf{V}\cdot\nabla)\mathbf{V} + 2\Omega\times\mathbf{V} + \frac{\partial\Omega}{\partial t}\times\mathbf{r} + \Omega\times(\Omega\times\mathbf{r}) = -\frac{1}{\rho}\nabla P + \nabla\phi_e, \tag{15}$$

where ρ denotes the core density here taken as homogeneous, P is the fluid pressure and ϕ_e denotes the exterior potential acting on the fluid. The vector field $\mathbf{V}$ denotes the velocity of the flow relative to the mantle. It can be safely treated as small compared to the uniform rotation at angular velocity Ω_0. For this reason, we can neglect the second term of eq. (15). This makes the remaining equation linear in the velocity, so that the flow response to tidal forcing can be analysed independently for each individual frequency. The flow velocity must satisfy the no-penetration condition at the CMB:

$$\hat{\mathbf{n}}\cdot\mathbf{V}|_{\rm cmb} = 0. \tag{16}$$

Wu & Wahr (1997) had the idea to separate the velocity field, $\mathbf{V}$, in two parts:

$$\mathbf{V} = \mathbf{v} + \mathbf{u}, \tag{17}$$

where the vector field $\mathbf{u}$ is treated as a small perturbation produced on the base flow, $\mathbf{v}$, by the non-hydrostatic CMB topography. Both fields must satisfy the incompressibility condition: $\nabla\cdot\mathbf{v} = \nabla\cdot\mathbf{u} = 0$. By using eq. (3), the momentum eq. (15), can then be split into two parts:

$$\frac{\partial\mathbf{v}}{\partial t} + 2\Omega_0\hat{\mathbf{z}}\times\mathbf{v} + \Omega_0\frac{\partial\mathbf{m}}{\partial t}\times\mathbf{r} - \nabla\phi_m = \nabla\chi, \tag{18}$$

$$\frac{\partial\mathbf{u}}{\partial t} + 2\Omega_0\hat{\mathbf{z}}\times\mathbf{u} + \nabla p = -\nabla\chi, \tag{19}$$

where we have introduced the reduced pressure p and the centrifugal potential ϕ_m, respectively defined as:

$$p = \tfrac{P}{\rho} - \phi_e, \tag{20}$$

$$\phi_m = -\tfrac{1}{2}|\Omega\times\mathbf{r}|^2 + \tfrac{1}{2}\Omega_0^2|\hat{\mathbf{z}}\times\mathbf{r}|^2, \tag{21}$$

where the second term of eq. (21) is the centrifugal potential at equilibrium.

The scalar function, χ, appearing in both eqs (18) and (19), cannot be uniquely determined so that the decomposition of eq. (15) is not unique. It is convenient to consider this decomposition so that the first part represents the flow motion without CMB topography. For LOD variations, we follow Wu & Wahr who have simply chosen $\chi = 0$, which indeed corresponds to the main tidal flow when ignoring the CMB topography. Eq. (18) may then be solved immediately for the base flow, $\mathbf{v}$, within the hydrostatic fluid core, once we know the axial component of $\mathbf{m}$, which is here given by eq. (8), giving:

$$\mathbf{v} = \Omega_0 \mathrm{m}_{f,3}^0\hat{\mathbf{z}}\times\mathbf{r}, \tag{22}$$

where $\mathrm{m}_{f,3}^0$ should be read from eq. (9). Neglecting the tidal deformation of the core, this solution simply reduces to $\mathbf{v} = -\Omega_0\mathrm{m}_{f,3}^0\hat{\mathbf{z}}\times\mathbf{r}$, which is the solution of the *spin-up* problem when there is no coupling at the CMB (Greenspan 1969).

The whole point of using the decomposition eq. (17) lies in the form of the dynamical eq. (19) for the perturbation, $\mathbf{u}$. Focusing on the flow response to a given tidal frequency, $\omega_{\rm tidal} = \sigma_m\Omega_0$, we may write $\mathbf{u} = \tilde{\mathbf{u}}e^{i\sigma_m\Omega_0 t}$, and $p = \tilde{p}e^{i\sigma_m\Omega_0 t}$. Eq. (19) may then be rewritten as:

$$\tilde{\mathbf{u}} = \frac{-i\sigma_m}{4-\sigma_m^2}\left(\nabla\tilde{p} - \frac{2}{i\sigma_m}\hat{\mathbf{z}}\times\nabla\tilde{p} - \frac{4}{\sigma_m^2}(\hat{\mathbf{z}}\cdot\nabla\tilde{p})\hat{\mathbf{z}}\right)\frac{1}{\Omega_0}. \tag{23}$$

Taking the divergence on both sides and using $\nabla.\mathbf{u} = 0$, we find:

$$\nabla^2 \tilde{p} - \frac{4}{\sigma_m^2}(\hat{\mathbf{z}} \cdot \nabla)^2 \tilde{p} = 0. \tag{24}$$

This is the *Poincaré equation* governing the dynamics of *inertial waves*. Analytical solutions to this equation can be written explicitly in terms of specially tailored bi-spheroidal coordinates for both the spherical and oblate spheroidal fluid core (Greenspan 1969; see also Rieutord 2014; Zhang & Liao 2017; and eq. (A13) of Rekier *et al.* 2019). For our purpose, we only need the general solution on the sphere located at the mean CMB radius, R, where it can be written as a spherical harmonics expansion (Wu & Wahr 1997):

$$\tilde{p}|_{r=R} = \sum_{\ell=1}^{\infty} \sum_{m=-\ell}^{\ell} a_\ell^m \; P_\ell^m \left(\frac{\sigma_m}{2}\right) Y_\ell^m(\theta, \lambda). \tag{25}$$

The above [combined with eq. (20)] can be used into eq. (14) to compute the pressure torque at the CMB. In the axial direction, this reads:

$$\Gamma_{\mathrm{cmb},3} = -i\,\Omega_0^2 R^5 \sum_{\ell=1}^{\ell_{\max}} \sum_{m=-\ell}^{\ell} (-1)^m m\, P_\ell^m \left(\frac{\sigma_m}{2}\right) \varepsilon_\ell^{-m} a_\ell^m. \tag{26}$$

The last step is to compute the values of the complex coefficients a_ℓ^m. This is done by inserting eq. (25) back into eq. (23) and using the boundary condition eq. (16) which, upon using eqs (17) and (22), reduces to:

$$\hat{\mathbf{n}} \cdot \left(\tilde{\mathbf{u}} + \Omega_0 \mathrm{m}_{f,3}^0 \hat{\mathbf{z}} \times \mathbf{r}\right)|_{r=R} = 0. \tag{27}$$

After some algebra (see also Appendix A), one finds:

$$a_\ell^m = -2 \frac{\left(1 - \frac{\sigma_m^2}{4}\right)}{[\dots]_\ell^m} m\, \varepsilon_\ell^m\, \mathrm{m}_{f,3}^0, \tag{28}$$

$$a_\ell^{-m} = 2 \frac{\left(1 - \frac{\sigma_m^2}{4}\right)}{[\dots]_\ell^{-m}} (-1)^m m\, \varepsilon_\ell^{m*}\, \mathrm{m}_{f,3}^0, \tag{29}$$

where $m > 0$, and we have introduced the following shorthand in the denominator:

$$[\dots]_\ell^m = \left[m P_\ell^m \left(\frac{\sigma_m}{2}\right) - \left(1 - \frac{\sigma_m^2}{4}\right) P_\ell^{m\prime} \left(\frac{\sigma_m}{2}\right)\right]. \tag{30}$$

where $'$ denotes the derivative and where $-l \leq m \leq l$. The values of σ_m for which this quantity appearing in the denominator of eqs (28) and (29) is zero correspond to the frequencies of the *inertial modes* of the rotating fluid sphere (Greenspan 1969). The above derivation shows that those modes can resonantly amplify the tidal variations in the LOD. We quantify this mechanism in the next section.

When actually computing ΔLOD based on eq. (7), it is useful to relate observations of ΔLOD at frequency σ_m to a reference chosen at a well-known frequency, e.g. the lunar fortnightly frequency of the tide M_f (period 13.66 d), far away from any resonance using:

$$\mathrm{m}_3^0(\sigma_m) = \mathrm{m}_3^0(\sigma_{M_f}) \, \frac{\phi^{ext}(\sigma_m)}{\phi^{ext}(\sigma_{M_f})}, \tag{31}$$

where ϕ^{ext} is the external tidal potential at a given frequency. Combining all the above, one has:

$$\Delta\mathrm{LOD}(\sigma_m) = \left(1 - \sum_{\ell=1}^{\ell_{max}} \sum_{m=-\ell}^{\ell} m^2 \, P_\ell^m \left(\frac{\sigma_m}{2}\right) \frac{2}{[\dots]_\ell^m \, \Omega_0^2 C_m} \, \varepsilon_\ell^m \, \varepsilon_\ell^{m*}\right) \frac{\phi^{ext}(\sigma_m)}{\phi^{ext}(\sigma_{M_f})} \, \Delta\mathrm{LOD}(\sigma_{M_f}) \tag{32}$$

3 RESONANT AMPLIFICATION IN TIDAL VARIATION OF LOD FROM TOPOGRAPHY

In order to estimate the amplitude of the resonance in the tidal ΔLOD, we need a model of the CMB topography. We use the topographic coefficients as measured by seismologists Morelli & Dziewonski 1987; Boschi & Dziewonski 2000; Sze & van der Hilst 2003; Simmons *et al.* 2009). These models are restricted to long-wavelength topography. CMB topography is thought to be primarily due to isostatic compensation of long-wavelength density anomalies in the lowermost mantle [see e.g. Dehant *et al.* (2022) for a review]. At this time, there is no convergence towards a global model of the bottom mantle anomalies to derive a topographic map of the CMB unambiguously. Although the topography models mostly show elevated topographies under the Pacific and Africa, implying a rather large degree 2-order 2 topography coefficient details differ between models. So, we decided not to use those dynamical models and to use the seismological models. The data are for the real $\epsilon_{c\,n}^m$ and $\epsilon_{s\,n}^m$ and are restricted to low degrees.

In order to test our analytical approach adequately, we want to use topographic coefficients of higher orders and degrees. We calculate these coefficients by using Kaula's rule (Kaula 1966), which predicts that gravity coefficients are inversely proportional to the square of the degree n. When applied to the CMB topography, this predicts $\varepsilon_n^m \sim n^{-2}$. This choice is consistent with the current knowledge relating topography and gravity coefficients (see e.g. Chao & Rubincam 1989 and Ermakov *et al.* 2018) since the CMB is an equipotential surface.

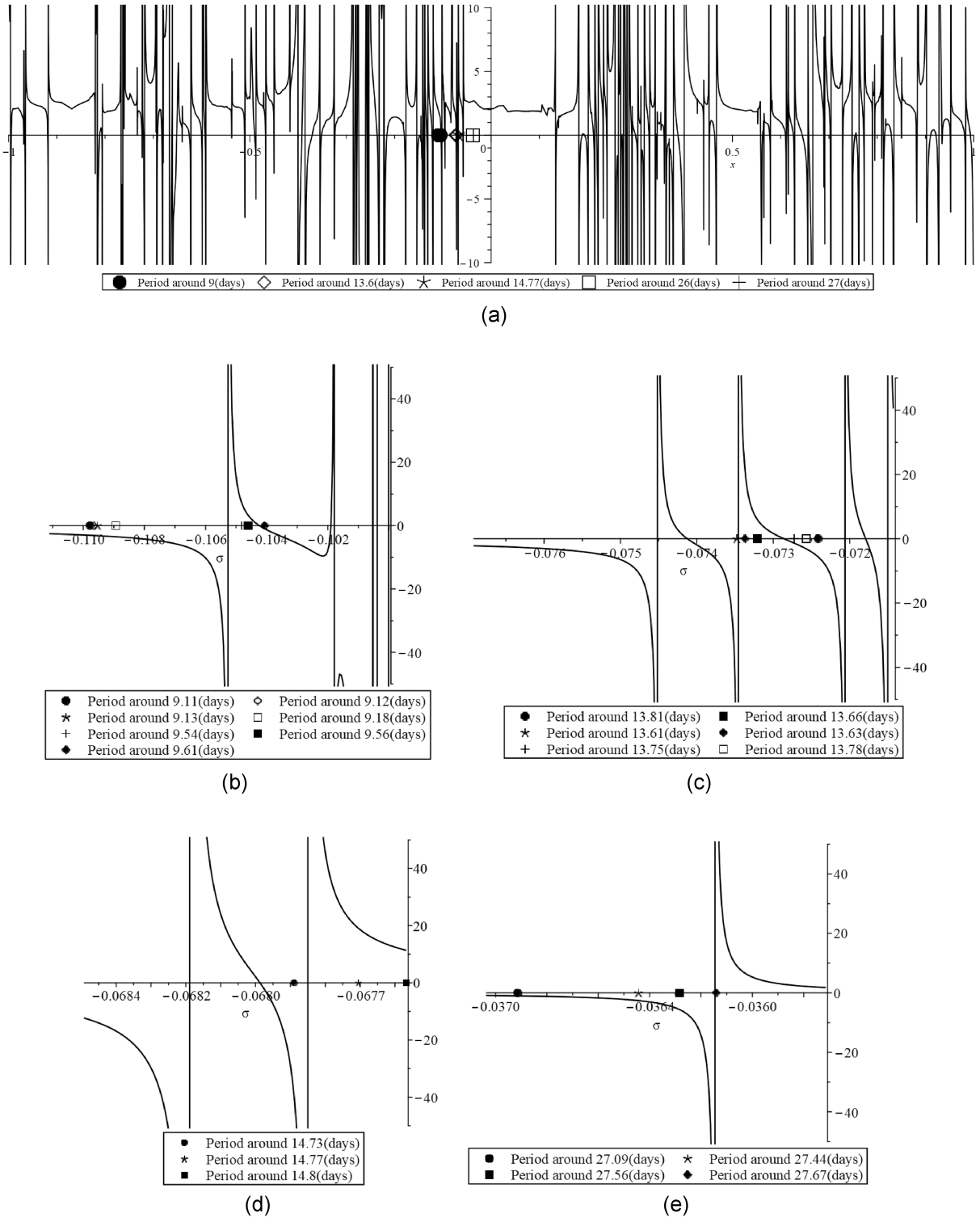

Figure 1. Resonances in the total torque (a); Zoom into the total torque around 9.61 d (b), 13.66 d (M_f tide) (c), 14.77 d (d) and 27 d (M_m tide) (e), which includes the largest resonantly affected tides.

We look for resonance frequencies that can be close to tidal frequencies corresponding to long-period tides. In practice, we search for the solutions of the equation $[...]_n^m = 0$ that lie in the frequency band $[-0.5, 0.5]$ cycle/d. These solutions refer to all periods larger than 2 d. The spectrum is divided in frequency bands with central periods near the tidal periods at 9.1, 9.18, 9.54, 9.61, 13.61, 13.66, 13.81, 14.19, 14.77, 26.88, 27.55 or 182.62 d. These resonances would amplify the total third component of the torque leading to enhanced LOD variations.

Fig. 1 shows the resonant behaviour of the total torque as a function of frequency. In Table 1, we identify those resonance periods near tidal periods, and we provide the amplification in ΔLOD. We do so by means of eq. (32). The amplification is proportional to the square of the

Table 1. Possible amplifications in tidal LOD variations

Central period (d)	(degree n, order m)	Resonance period (d)	Tidal period (d)	Amplification (normalized on M_f)
9.61	(6,2)	9.8241	9.8736	$2.4\cdot(\varepsilon_6^2)^2$
13.81	(9,3)	13.9857	13.7773	$51.6\cdot(\varepsilon_9^3)^2$
14.77	(5,1)	14.6651	14.6981	$2.6\cdot(\varepsilon_5^1)^2$
			14.6664	$10.5\cdot(\varepsilon_5^1)^2$
27.55 (M_m)	(7,1)	27.6658	27.5545	$816.5\cdot(\varepsilon_7^1)^2$
			27.6668	$5963.3\cdot(\varepsilon_7^1)^2$
13.66 (M_f)	(18,10)	13.6136	13.6333	$15568.8\cdot(\varepsilon_{18}^{10})^2$
14.77	(15,7)	14.7384	14.7653	$1923.3\cdot(\varepsilon_{15}^7)^2$
182.62 (S_{Sa})	(19,1)	189.6665	189.6211	$75.7\cdot(\varepsilon_{19}^7)^2$

associated topography ε_n^m, and the amplification factor can be several orders of magnitude larger than 1. For example, the ΔLOD associated with the tide at 27.6668 d, quite close to a resonance, is amplified by $5963.3(\varepsilon_7^1)^2$.

As seen from the last column of Table 1, there is a large range of amplification factors in front of the normalized topography coefficients. The maximum amplification factor is for the tide at 13.6333 d near the M_f tide with an amplification at the level of $15569(\varepsilon_{18}^{10})^2$. Since ε_{18}^{10}, according to the Kaula rule, is small, of the order of $5\,10^{-3}$, the amplification is 0.06 ms. Considering that the LOD variation at the tidal period of 13.6333 d (see chapter 8 of IERS Standard) is 0.15 ms (millisecond), as theoretically computed from Defraigne and Smith (1999), the total amplitude could, therefore, increase to 0.21 ms and the observed residuals (between 0.02 and 0.11 ms) could be explained (Kouba and Vondrák 2005; Vondrák and Ron, 2005; Shen and Peng 2016; Dill *et al.* 2019).

The lowest degree topography that can induce a resonance in the tidal effects on LOD is degree 5. The amplification for the tide at 14.6664 d is only a factor of $10.5(\varepsilon_5^1)^2$. The LOD variation associated with that tide is very small.

There is a resonance frequency very near the M_m tide at 27.666 d, which influences the tides at 27.55 d as well as at 27.667 d. The amplifications are respectively $817(\varepsilon_7^1)^2$ and $5963(\varepsilon_7^1)^2$. As ε_7^1 can be of the order of 0.02, the tide at 27.55 d can be amplified 2.4 times and the associated LOD variations would be of the order of 0.03 ms, depending on the effective value of ε_7^1. Similarly, the tide at 27.67 d can be amplified 0.3 times and the associated LOD variations would be of the order of 0.06 ms. This amplification is similar to the one of the M_f tide. Both contributions around 27.7 d combined would provide a spectral amplitude that is a little bit too high compared to the observation residuals ranging from 0.02 to 0.03 ms.

4 DISCUSSION

The focus of the current research is on quantifying the response of the Earth's rotation to tidal forcing when considering a topography at the CMB. In order to achieve this goal, we have developed an analytical approach for solving the Navier–Stokes equation for global rotational motions plus inertial waves, based on and extending the approach of Wu & Wahr (1997). From their numerical solution for a topography up to degree 6, they concluded that the effect of a topographic torque on the LOD variation is very small. We have revisited the computations and considered a completely analytical method. The advantage of our analytical method is that it allows us to directly identify the frequencies and topographic degrees and orders where resonances can happen. At these frequencies, the LOD variations can be amplified as seen from Fig. 1.

We extended the computation of the topographic torque to higher degrees and orders than 6 [the maximum used in Wu & Wahr (1997)]. Since many of the topographic coefficients are not observed at the CMB, we have assumed that they follow the Kaula rule, similar to that of the gravity field. We have estimated the coefficients of such a law using the observed values of the CMB coefficients at low degrees and orders and used these coefficients to extrapolate to higher orders and degrees. This provided us with an order of magnitude of what we can expect. We have computed the resonances for these degrees and orders, as well as the maximum amplifications near the tidal frequencies given by the tide generating potential.

From our analysis, we have shown that the conclusion in Wu & Wahr (1997) on very small LOD contributions due to the effects of topography still holds when considering higher degrees and orders. However, Wu & Wahr (1997) have small contributions at the microsecond level in the tidal effects on LOD considered (see their table 6). We have demonstrated that the tide at 13.63 d near M_f and the tide at 27.56 d near M_m can both be amplified by 0.06 ms based on a mean topography. Observations from VLBI and GNSS combined show some residuals ranging from 0.02 to 0.11 ms near the 13.63 d tide and from 0.02 to 0.03 ms near the 27.7 d tide (Kouba and Vondrák 2005; Vondrák and Ron 2005; Shen and Peng 2016; Dill *et al.* 2019). It is tempting to suggest that topographic coupling might explain these residuals, although the IERS Earth rotation parameters around the semi-diurnal and diurnal periods are not perfectly corrected for the ocean tides. Errors in the determination of the tiny semi-diurnal constituents OP_2 and λ_2 could be aliased into M_f and M_m, respectively (Woodworth & Hibbert 2018).

Our analysis concentrated on the topographic coupling at the CMB and did not consider other CMB coupling mechanisms and the presence of an inner core. Zhang (1992) and Zhang & Liao (2017) showed that inertial waves (appearing in our computation) with a small azimuthal wave number are only weakly modified by an inner core (see also Triana *et al.* 2022). Since the largest effects are associated with small azimuthal wave number, we expect the inner core to have a negligible effect on our results. The introduction of neglected additional

CMB couplings into Liouville eq. (2) would only slightly change the amplitude of the unperturbed wobble, m_3^0, to leading order in the CMB flattening. Nevertheless, even though the electromagnetic force is dominated by inertia at the timescales considered, its presence can slightly alter the frequency of inertial modes in the core, possibly pushing them into or away from resonance (Luo and Jackson, 2022; Luo *et al.* 2022). Moreover, introducing viscous and ohmic dissipation into the model causes inertial modes to become damped, which can slightly reduce the amplification.

ACKNOWLEDGMENTS

The research leading to these results has received funding from the European Research Council under ERC advanced grant 670874 (RotaNut - Rotation and Nutation of a wobbly Earth), as well as ERC synergy grant 855677 (GRACEFUL - Gravimetry, magnetism and core flow). Also, the Belgian Fund for Scientific Research FNRS-FRS is acknowledged for its financial support through the research project number PDR T.0066.20 at UCLouvain.

We would like also to acknowledge Jim Ray for precious advises and, as well as Felix Gerick, Santiago Andres Triana, Antony Trinh and Sheng-An Shih for interesting discussions.

We would like to deeply thank Ben Fong Chao and an anonymous reviewer for their constructive review, as well as the editor Bert Vermeersen.

DATA AVAILABILITY STATEMENT

The data (topographic spherical harmonic coefficients at the CMB) underlying this article are available (a few numbers) in Boschi & Dziewonski (2000); Morelli & Dziewonski (1987); Simmons *et al.* (2009); and Sze & van der Hilst (2003). These data sets were thus derived from following sources:

Boschi & Dziewonski (2000): https://doi.org/10.1029/2000JB900059,
Morelli & Dziewonski (1987): https://doi.org/10.1038/325678a0,
Simmons *et al.* (2009): https://doi.org/10.1111/j.1365-246X.2009.04133.x,
Sze & van der Hilst (2003): https://doi.org/10.1016/S0031-9201(02)00204-2.

REFERENCES

Asari, S. & Wardinski, I., 2015. On magnetic estimation of Earth's core angular momentum variation, *J. geophys. Res.: Solid Earth,* **120,** 6740–6757.

Aubert, J. & Gillet, N., 2021. The interplay of fast waves and slow convection in geodynamo simulations nearing Earth's core conditions, *Geophys. J. Int.,* **225**(3), 1854–1873.

Böhm, J., Hobiger, T., Ichikawa, R. & Koyama, Y., 2010. Asymmetric tropospheric delays from numerical weather models for UT1 determination from VLBI Intensive sessions on the baseline Wettzell-Tsukuba, *J. Geod.,* **84,** 319–325.

Boschi, L. & Dziewonski, A.M., 2000. Whole Earth tomography from delay times of P, PcP, PKP phases: lateral heterogeneities in the outer core, or radial anisotropy in the mantle, *J. geophys. Res.,* **105,** 13675–13969.

Buffett, B.A., 1996. A mechanism for decade fluctuations in the length of day, *Geophys. Res. Lett.,* **23**(25), 3803–3806.

Chao, B.F. & Rubincam, D.P., 1989. The gravitational field of Phobos, *Geophys. Res. Lett.,* **16,** 859–862.

Chen, J., 2005. Global mass balance and the length-of-day variation, *J. geophys. Res.,* **110,** B08404. doi:10.1029/2004JB003474.

Chen, J., Wilson, C.R. & Chao, B.F., 2019. Interannual oscillations in Earth rotation, *J. geophys. Res.,* **124**(12), 13404–13414.

Defraigne, P. & Smits, I., 1999. Length of day variations due to zonal tides for an inelastic Earth in non-hydrostatic equilibrium, *Geophys. J. Int.,* **139,** 563–572.

Dehant, V. & Mathews, P.M., 2015. Precession, Nutation and Wobble of the Earth, pp. 536, Cambridge University Press, ISBN:9781107092549.

Dehant, V., Trønnes, R.G., Campuzano, S.A., De Santis, A. & van Westrenen, W., 2022. Structure, materials and processes in the Earth's core and mantle, *Surveys Geophys.,* **43**(1), 263–302 . in S.I.: 'Probing Earth's Deep Interior using Space Observations Synergistically' . doi:10.1007/s10712-021-09684-y.

Dill, R. & Dobslaw, H., 2019. Seasonal variations in global mean sea level and consequences on the excitation of length-of-day changes, *Geophys. J. Int.,* **218**(2), 801–816.

Dill, R., Dobslaw, H. & Thomas, M., 2019. Improved 90-day Earth orientation predictions from angular momentum forecasts of atmosphere, ocean, and terrestrial hydrosphere, *J. Geod.,* **93,** 287–295.

Ermakov, A.I., Park, R.S. & Bills, B.G., 2018. Power laws of topography and gravity spectra of the solar system bodies, *J. geophys. Res.: Planets,* **123,** 2038–2064.

Gerick, F., Jault, D., Noir, J. & Vidal, J., 2020. Pressure torque of torsional Alfvén modes acting on an ellipsoidal mantle, *Geophys. J. Int.,* **222**(1), 338–351.

Gillet, N., Jault, D., Canet, E. & Fournier, A., 2010. Fast torsional waves and strong magnetic field within the Earth's core, *Nature,* **465,** 74–77.

Gillet, N., Jault, D. & Canet, E., 2017. Excitation of travelling torsional normal modes in an Earth's core model, *Geophys. J. Int.,* **210**(3), 1503–1516.

Gillet, N., Jault, D. & Canet, E., 2019. Excitation of travelling torsional normal modes in an Earth's core model, *Geophys. J. Int.,* **210,** 1503–1516.

Gillet, N., Gerick, F., Jault, D., Schwaiger, T., Aubert, J. & Istas, M., 2022a. Satellite magnetic data reveal interannual modes in Earth's core., *Proc. Natl. Acad. Sci,* **119**(13), E2115258119 . doi:10.1073/pnas.2115258119.

Gillet, N., Gerick, F., Angappan, R. & Jault, D., 2022b. A Dynamical Prospective on Interannual Geomagnetic Field Changes., *Surveys Geophys.,* **43,** 71–105.

Greenspan, H.P., 1969. *The Theory of Rotating Fluids,* Cambridge University Press, ISBN 10: 0521051479, ISBN 13: 9780521051477, 340 pages.

Greiner-Mai, H., Jochmann, H., Barthelmes, F. & Ballani, L., 2003. ossible influences of core processes on the Earth's rotation and the gravity field, *J. Geodyn.,* **36**(3), 343–358.

Hide, R., 1969. Interaction between the Earth's liquid core and solid mantle, *Nature,* **222,** 1055–1056.

Hide, R., 1989. Fluctuations in the Earth's rotation and the topohraphy of the core-mantle interface, *Phil. Trans. R. Soc. Lond., A,* **328,** 351–363.

Hide, R., Clayton, R.W., Hager, B.H, Spieth, M.A. & Voorhies, C.V., 1993. Topographic Core-Mantle Coupling and Fluctuations in the Earth's Rotation, *Geophysical Monograph Series, Relating Geophysical Structures and Processes: The Jeffreys Volume, Chapter 8,* pp. 107–120, ISBN: 9780875904672, doi: 10.1029/GM076p0107.

Jault, D. & Le Mouël, J.-L., 1989. The topographic torque associated with a tangentially geostrophic motion at the core surface and inferences on the flow inside the core, *Geophys. astrophys. Fluid. Dyn.,* **48,** 273–296.

Jault, D. & Le Mouël, J.-L., 1990. Core-mantle boundary shape: constraints inferred from the pressure torque acting between the core and the mantle, *Geophys. J. Int.,* **101,** 233–241.

Jin, S., Zhang, L.J. & Tapley, B.D., 2011. The understanding of length-of-day variations from satellite gravity and laser ranging measurements, *Geophys. J. Int.,* **184,** 651–660.

Kaula, W.M., 1966. *Theory of Satellite Geodesy,* Publ. Blaisdell, Waltham.

Kouba, J. & Vondrák, J., 2005. Comparison of length of day with oceanic and atmospheric angular momentum series, *J. Geod.,* **79,** 256–268.

Kuang, W. & Bloxham, J., 1993. On the effect of boundary topography on flow in the Earth's core, *Geophys. astrophys. Fluid. Dyn.,* **72**(1–4), 161–195.

Kuang, W. & Chao, B.F., 2001. Topographic core-mantle coupling in geodynamo modelling, *Geophys. Res. Lett.,* **28**(9), 1871–1874.

Lambert, S.B., Marcus, S.L. & de Viron, O., 2017. Atmospheric torques and Earth's rotation: what drove the millisecond-level length-of-day response to the 2015-2016 El Niño?, *Earth Syst. Dyn.,* **8,** 1009–1017.

Landskron, D. & Böhm, J., 2019. Improving dUT1 from VLBI intensive sessions with GRAD gradients and ray-traced delays, *Adv. Space Res.,* **63**(11), 3429–3435.

Luo, J. & Jackson, A., 2022. Waves in the Earth's core. I. Mildly diffusive torsional oscillations, *Proc. R. Soc. A,* **478,** 20210982. doi:10.1098/rspa.2021.0982.

Luo, J., Marti, P. & Jackson, A., 2022. Waves in the Earth's core. II. Magneto-Coriolis modes, *Proc. R. Soc. A,* **478,** 20220108. doi:10.1098/rspa.2022.0108.

Marcus, S.L., Dickey, J.O., Fukumori, I. & de Viron, O., 2012. Detection of the Earth rotation response to a rapid fluctuation of Southern Ocean circulation in November 2009, *Geophys. Res. Lett.,* **39,** L04605. doi:10.1029/2011GL050671.

Mathews, P.M., Buffett, B.A., Herring, T.A. & Shapiro, I.I., 1991a. Forced nutations of the Earth: Influence of inner core Dynamics. I. Theory, *J. geophys. Res.,* **96**(B5), 8219–8242.

Mathews, P.M., Buffett, B.A., Herring, T.A. & Shapiro, I.I., 1991b. Forced nutations of the Earth: Influence of inner core Dynamics. II. Numerical results and comparisons, *J. geophys. Res.,* **96**(B5), 8243–8258.

Mathews, P.M., Herring, T.A. & Buffett, B.A., 2002. Modelling of nutation and precession: new nutation series for non-rigid Earth and insights into the Earth's interior, *J. geophys. Res.,* **107**(B4), CI:2068. doi:10.1029/2001JB000390.

Morelli, A. & Dziewonski, M.A., 1987. Topography of the core-mantle boundary and lateral homogeneity of the liquid core, *Nature,* **325,** 678–683.

Mound, J.E. & Buffett, B.A., 2003. Interannual oscillations in length of day: implications for the structure of the mantle and core, *J. geophys. Res.,* **108**(B7), 2334. doi:10.1029/2002JB002054.

Ray, J., Griffiths, J., Collilieux, X. & Rebischung, P., 2013. Subseasonal GNSS positioning errors, *Geophys. Res. Lett.,* **40**(22), 5854–5860.

Rebischung, P., Altamimi, Z., Ray, J. & Garayt, B., 2016. The IGS contribution to ITRF2014, *J. Geod.,* **90**(7), 611–630.

Rekier, J., Trinh, A., Triana, S.A. & Dehant, V., 2019. Inertial modes in near-spherical geometries, *Geophys. J. Int.,* **216**(2), 777–793.

Rekier, J., Trinh, A., Triana, S.A. & Dehant, V., 2020. Inertial modes of a freely rotating ellipsoidal planet and their relation to nutations, *Planet. Sci. J.,* **1**(1), Id.20. doi:10.3847/PSJ/ab93c8.

Rieutord, M., 2014. *Une introduction à la dynamique des fluides,* ed. de Boeck, SUP, 1st Edition, pages 504. ISBN2804185540.

Sasao, T., Okubo, S. & Saito, M., 1980. A simple theory on the dynamical effects of a stratified fluid core upon nutational motion of the Earth, in *"Nutation and the Earth's rotation", Proc. IAU Symposium,* pp. 165–183, D. Reidel Publishing, Co., Dordrecht. Kiev, Ukrainian SSR 1977.

Senior, K., Kouba, J. & Ray, J., 2010. Status and Prospects for Combined GPS LOD and VLBI UT1 Measurements, *Artificial Satellites,* **45**(2), 57–73.

Shen, W. & Peng, C., 2016. Detection of different-time-scale signals in the length of day variation based on EEMD analysis technique, *Geod. Geodyn.,* **7**(3), 180–186.

Simmons, N., Forte, A. & Grand, S., 2009. Joint seismic, geodynamic and mineral physical constraints on three-dimensional mantle heterogeneity: Implications for the relative importance of thermal versus compositional heterogeneity, *Geophys. J. Int.,* **177,** 1285–1304.

Sze, E. & van der Hilst, R., 2003. Core mantle boundary topography from short period PcP, PKP and PKKP data, *Phys. Earth planet. Inter.,* **135,** 27–46.

Teed, R.J., Jones, C.A. & Tobias, S.M., 2018. Torsional waves driven by convection and jets in Earth's liquid core, *Geophys. J. Int.,* **216**(1), 123–129.

Triana, S.A., Dumberry, M., Cébron, D., Vidal, J., Trinh, A., Gerick, F. & Rekier, J., 2022. Core eigenmodes and their impact on the Earth's rotation, *Surv. Geophys.,* **43,** 107–148.

Vondrák, J. & Ron, C., 2005. Combining GPS and VLBI measurements of celestial motion of the Earth's spin axis and universal time, *Acta Geodyn. Geomater.,* **2**(3), 87–94 . Id. 139.

Wahr, J.M., 1981. The forced nutations of an elliptical, rotating, elastic and oceanless earth, *Geophys. J. R. astr. Soc.,* **64,** 105–121.

Watkins, A., Fu, Y. & Gross, R., 2018. Earth's subdecadal angular momentum balance from deformation and rotation data, *Sci. Rep.,* **8,** 13761. doi:10.1038/s41598-018-32043-8.

Woodworth, P.L. & Hibbert, A., 2018. The nodal dependence of long-period ocean tides in the Drake Passage, *Ocean Sci.,* **14,** 711–730.

Wu, X. & Wahr, J.M., 1997. Effects of non-hydrostatic core-mantle boundary topography and core dynamics on Earth rotation, *Geophys. J. Int.,* **128**(1), 18–42.

Yoshida, S. & Hamano, Y., 1993. The westward drift of the geomagnetic field caused by length-of-day variation, and the topography of the core-mantle boundary, *Geophys. J.,* **114**(3), 696–710.

Yoshida, S. & Hamano, Y., 1995. Geomagnetic decadal variations caused by length-of-day variation, *Phys. Earth planet. Inter.,* **91**(1–3), 117–129.

Zatman, S. & Bloxham, J., 1997. Torsional oscillations and the magnetic field within the Earth's core, *Nature,* **388,** 760–763.

Zatman, S. & Bloxham, J., 1999. On the dynamical implications of models of Bs from torsional oscillations of the Earth's core, *Geophys. J. Int.,* **138,** 679–686.

Zhang, K., 1992. On inertial waves in the Earth's fluid core, *Geophys. Res. Lett.,* **19**(8), 737–740.

Zhang, K. & Liao, X., 2017. *Theory and Modeling of Rotating Fluids: Convection, Inertial Waves and Precession,* Cambridge University Press, Cambridge Monographs on Mechanics, 1st Edition, ISBN 9781139024853, 526 pages. doi: 10.1017/9781139024853.

Zhou, Y.H., Salstein, D.A. & Chen, J.L., 2006. Revised atmospheric excitation function series related to Earth's variable rotation under consideration of surface topography, *J. geophys. Res. Atmospheres,* **111**(D12), CiteIDD12108. doi:10.1029/2005JD006608.

APPENDIX A: COEFFICIENTS a_l^k OF THE TORQUE

Expressions for the a_l^k coefficients of the torque can be obtained by applying the boundary condition eq. (16) to **u** and **v**. We take **u** from eq. (19) with Φ provided by eq. (20). We also take **v** from eq. (22). The resulting expression corresponds to the expression $(B4) - (B12) = 0$

in the appendix of Wu & Wahr (1997) and is of the form:

$$\sum_{l,k} Y_l^k \left[k P_l^k \left(\frac{\sigma_m}{2}\right) - \left(1 - \frac{\sigma_m^2}{4}\right) P_l^{k\prime} \left(\frac{\sigma_m}{2}\right) \right] a_l^k \; - \; 2\left(1 - \frac{\sigma_m^2}{4}\right) \sum_{n=1,m} m \varepsilon_n^m Y_n^m \; m_3 \; = \; 0. \tag{A1}$$

eq. (A1) allows us to obtain analytical expressions for the coefficients a_l^k as a function of ε_n^m at each frequency of interest. We first multiply eq. (A1) by the complex conjugate of the spherical harmonics Y_n^m, integrate over 2π and apply the orthonormality condition. We then obtain a much easier form of eq. (A1) relating a_n^m linearly with ε_n^m for each n and m:

$$\left[m P_n^m \left(\frac{\sigma_m}{2}\right) - \left(1 - \frac{\sigma_m^2}{4}\right) P_n^{m\prime} \left(\frac{\sigma_m}{2}\right) \right] a_n^m = 2\left(1 - \frac{\sigma_m^2}{4}\right) m \varepsilon_n^m \; m_3. \tag{A2}$$

Using eq. (B9), we also have

$$\left[(-m) P_n^{-m} \left(\frac{\sigma_m}{2}\right) - \left(1 - \frac{\sigma_m^2}{4}\right) P_n^{-m\prime} \left(\frac{\sigma_m}{2}\right) \right] a_n^{-m} = 2\left(1 - \frac{\sigma_m^2}{4}\right) (-m)(-1)^m \varepsilon_n^{m*} \; m_3. \tag{A3}$$

For writing simplicity, we express the terms in brackets in eqs (A2) and (A3) as:

$$[...]_l^k = \left[k P_l^k \left(\frac{\sigma_m}{2}\right) - \left(1 - \frac{\sigma_m^2}{4}\right) P_l^{k\prime} \left(\frac{\sigma_m}{2}\right) \right] \tag{A4}$$

as already mentioned in eq. (30) and (for positive k)

$$[...]_l^{-k} = \left[-k P_l^{-k} \left(\frac{\sigma_m}{2}\right) - \left(1 - \frac{\sigma_m^2}{4}\right) P_l^{-k\prime} \left(\frac{\sigma_m}{2}\right) \right]. \tag{A5}$$

While combining negative and positive orders of the spherical harmonics for the ε_n^m provides a real topography, it must be noted that the combination of a_n^m and a_n^{-m} is not real due to the $(-m)$ coefficients appearing in eq. (A3). Therefore, Φ is a complex-valued for $m \neq 0$.

The case when $m = 0$ in eq. (A2) can be treated separately. The right-hand side of eqs (A2) and (A3) is equal to zero, and the coefficient a_n^m do not depend on the topographic amplitude. Indeed, this makes sense since with a zonal topography it is impossible to induce a zonal velocity.

The system of eqs (A2) and (A3) is undetermined when $[...]_n^m$ is equal to zero. This expresses an eigenvalue equation for σ_m and determines the condition for resonances to happen. In this case, it is impossible to determine a_n^m but we can determine the resonance frequencies, which do not depend on the topographic amplitudes.

Using eqs (A2) and (A3), we can straightforwardly express $a_n^{\pm m}$ in terms of the topographic coefficients $\varepsilon_n^{\pm m}$:

$$a_n^m = \frac{2\left(1 - \frac{\sigma_m^2}{4}\right)}{[...]_n^m} \; m \; \varepsilon_n^m \; m_3 \tag{A6}$$

and for the negative case:

$$a_n^{-m} = \frac{2\left(1 - \frac{\sigma_m^2}{4}\right)}{[...]_n^{-m}} \; (-m)(-1)^m \varepsilon_n^{m*} \; m_3 \tag{A7}$$

Eqs (A6) and (A7) show resonance effects when the denominators are equal to zero. The frequencies corresponding to $[...]_l^{\pm k} = 0$ given by eqs (A4) and (A5) are the inertial mode frequencies.

Besides depending linearly on ε_n^m, the coefficients a_n^m are also proportional to m_3 (or to m_3^0 to first order in the small quantities such as m_3^0, m_3).

APPENDIX B: EXPRESSION OF THE TOPOGRAPHY AT THE CORE-MANTLE BOUNDARY

Since rotation flattens the Earth, the coefficient $\varepsilon_{c\,2}^0$ contains a hydrostatic part next to a non-hydrostatic contribution to the topography:

$$\varepsilon_{c\,2}^0 = \varepsilon_{c\,2\,hydr.\,part}^0 + \varepsilon_{c\,2\,non-hydr.\,part}^0. \tag{B1}$$

The additional topography at the CMB with respect to the flattened core can thus be separated from the hydrostatic part as

$$r_{CMB} = R\left[1 + \varepsilon_{c\,2\,hydr.\,part}^0 P_2^0(\theta) + \sum_{n=1}^{N} \sum_{m=-n}^{m=n} (\varepsilon_{c\,n}^m \cos m\lambda + \varepsilon_{s\,n}^m \sin m\lambda) P_n^m(\theta) \right] \tag{B2}$$

where $\varepsilon_{c\,n}^m$ represent henceforth the non-hydrostatic contributions to the topography.

Note that for simplicity, we have kept the same notation for $\varepsilon_{c\,2}^0$.

The topographical coefficients and the spherical harmonics [as given by eq. (13)] can be related through a series of properties:

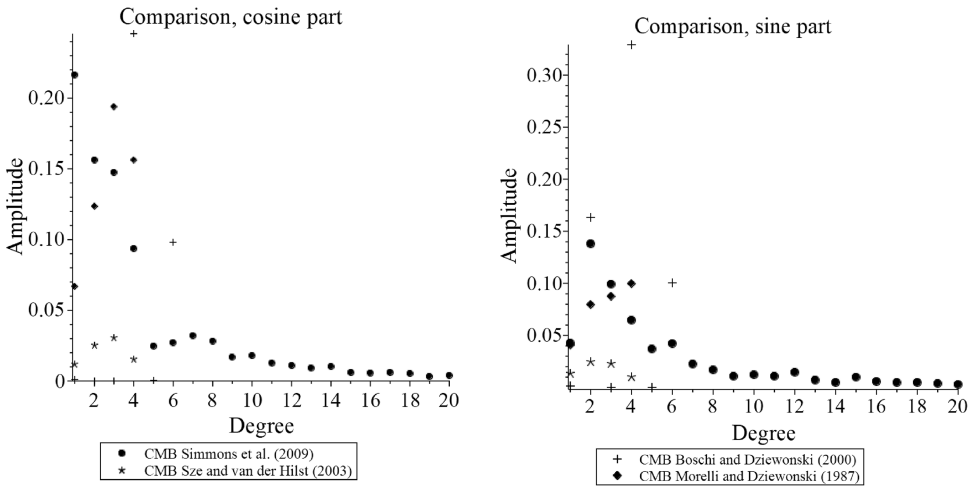

Figure A1. Topographic coefficients averaged over the orders and showing a decreasing law as a function of their degrees in their SH expansions.

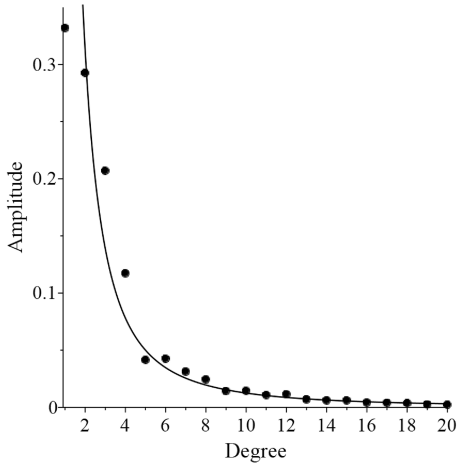

Figure A2. Topographic coefficient fitting according to Kaula's law. The dots are the mean of all orders as well as of all observation data sets.

$$\Re(\varepsilon_n^m) = \frac{\sqrt{2\pi}}{2}\varepsilon_{c\,n}^m \tag{B3}$$

$$\Re(\varepsilon_n^{-m}) = \frac{(-1)^m\sqrt{2\pi}}{2}\varepsilon_{c\,n}^m \tag{B4}$$

$$\Im(\varepsilon_n^m) = \frac{-\sqrt{2\pi}}{2}\varepsilon_{s\,n}^m \tag{B5}$$

$$\Im(\varepsilon_n^{-m}) = \frac{(-1)^m\sqrt{2\pi}}{2}\varepsilon_{s\,n}^m \tag{B6}$$

$$\varepsilon_n^m = \frac{\sqrt{2\pi}}{2}(\varepsilon_{c\,n}^m - i\varepsilon_{s\,n}^m) \tag{B7}$$

$$\varepsilon_n^{-m} = \frac{(-1)^m\sqrt{2\pi}}{2}(\varepsilon_{c\,n}^m + i\varepsilon_{s\,n}^m). \tag{B8}$$

where $\Re$ and $\Im$ are the real and imaginary part of a complex number, respectively.

In addition, since

$$\varepsilon_n^{-m} = (-1)^m\varepsilon_n^{m*}, \tag{B9}$$

we have

$$\varepsilon_n^{-m}Y_n^{-m}(\theta,\lambda) = \varepsilon_n^{m*}Y_n^{m*}(\theta,\lambda) \tag{B10}$$

and r_{CMB} given by eq. (12) is real.

APPENDIX C: KAULA RULE FOR THE TOPOGRAPHY COEFFICIENTS

In order to construct the topography coefficients, we proceed in several steps.

First of all, we brought the four sources of CMB topography to a common ground by scaling by the CMB mean radius. Fig. A1 depicts the coefficients obtained after this operation.

Furthermore, we have computed an average for the different cosine and sine coefficients for each given degree as provided by four sources (Morelli & Dziewonski 1987; Boschi & Dziewonski 2000; Sze & van der Hilst 2003; Simmons *et al.* 2009). We interpolate the obtained values to get a_s and a_c in Kaula's law. This states that that gravity coefficients are inversely proportional to the square of the degree n. By the same token, we consider that the approximation of the amplitude coefficients of the topography follows a function of the type $x \rightarrow \frac{a}{x^2}$ (Kaula 1966).

Consequently, we can extrapolate and obtain topography coefficients for any degree or order. See Fig. A2 for the coefficients thus obtained.